frontiers in Microbiology

TYPE Original Research
PUBLISHED 02 November 2026
DOI 10.3389/fmicb.2026.1891476

Check for updates

OPEN ACCESS

EDITED BY
Srdjan Stanković,
University of Belgrade, Serbia

REVIEWED BY
Chao Peng,
China West Normal University, China
Asmaa A. Halema,
Cairo University, Egypt

*CORRESPONDENCE
Qiyu Gao
gaog345@163.com
Guangcui Xu
xugc166@163.com

RECEIVED 26 May 2026
REVISED 08 July 2026
ACCEPTED 28 July 2026
PUBLISHED 02 November 2026

CITATION
Gao Q, Wang W, Xu L, Yang L, Wang J and Xu G (2026) Multi-omics reveals the response and adaptation of *Acidithiobacillus ferrooxidans* BY-3 under arsenic stress.
Front. Microbiol. 17:1891476.
doi: 10.3389/fmicb.2026.1891476

COPYRIGHT
© 2026 Gao, Wang, Xu, Yang, Wang and Xu. This is an open-access article distributed under the terms of the Creative Commons Attribution License (CC BY). The use, distribution or reproduction in other forums is permitted, provided the original author(s) and the copyright owner(s) are credited and that the original publication in this journal is cited, in accordance with accepted academic practice. No use, distribution or reproduction is permitted which does not comply with these terms.

Multi-omics reveals the response and adaptation of *Acidithiobacillus ferrooxidans* BY-3 under arsenic stress

Qiyu Gao[1,2]*, Wanting Wang[1], Lin Xu[1], Lan Yang[1], Jingyao Wang[1] and Guangcui Xu[3]*

[1]Synthetic Biology Engineering Lab of Henan Province, School of Life Science and Technology, Henan Medical University, Xinxiang, China, [2]Gansu Key Laboratory of Biomonitoring and Bioremediation for Environmental Pollution, Institute of Microbiology, School of Life Sciences, Lanzhou University, Lanzhou, China, [3]School of Public Health, Henan Medical University, Xinxiang, China

Acidithiobacillus ferrooxidans (*A. ferrooxidans*) exhibits strong arsenic resistance and plays a pivotal role in biometallurgy and sulfur cycling in ecosystems. In this study, integrated transcriptomic, proteomic, and metabolomic analyses were employed to elucidate the molecular response mechanisms of *Acidithiobacillus ferrooxidans* BY-3 (*At. f* BY-3) under arsenic stress. The study also evaluated its capacity for heavy metal bioleaching and provided new insights into bioremediation applications. Transcriptomic profiling revealed that the number of differentially expressed genes increased in an arsenic dose-dependent manner. Under arsenic stress, *At. f* BY-3 displayed global downregulation of genes involved in secondary metabolism and chemotaxis, thereby reducing unnecessary energy expenditure and reallocating metabolic resources toward arsenic resistance. Proteomic analysis identified 337 significantly differentially abundant proteins, which were primarily enriched in c-di-GMP signal transduction, sulfur cycling, redox homeostasis, and transmembrane transport. Metabolomic analysis detected 53 differential metabolites that were mainly associated with ABC transport systems, sulfur metabolism, and stress signaling pathways. Multi-omics integration demonstrated that *At. f* BY-3 maintained energy homeostasis through coordinated carbon and sulfur metabolism, enhanced arsenic efflux via activation of ABC transporters, and optimized membrane structure and signaling systems for improved stress perception. Sulfur cycling emerged as the central adaptive strategy for arsenic resistance. Furthermore, bioleaching assays confirmed the robust arsenic bioleaching capability of *At. f* BY-3, which was further enhanced following domestication. Overall, this work clarifies the molecular mechanisms underlying arsenic resistance in *A. ferrooxidans*, providing a theoretical foundation for optimizing biohydrometallurgy processes and heavy metal bioremediation strategies.

KEYWORDS
***Acidithiobacillus ferrooxidans*, arsenic, bioleaching, metabolomic, proteomic, transcriptomic**

1 Introduction

Microorganisms play an indispensable role in maintaining ecological balance and driving key biogeochemical cycles in Earth's ecosystems (Coleine et al., 2025; Rosenberg and Zilber-Rosenberg, 2022; Wu et al., 2024). *Acidithiobacillus ferrooxidans*

(*A. ferrooxidans*) is a chemolithoautotrophic bacterium that thrives in extreme acidic environments, including acid mine drainage (AMD), seawater, volcanic ash, and iron- or sulfur-rich acidic habitats (Kato et al., 2022; Li et al., 2014; Wang et al., 2025). Owing to its unique physiological characteristics, *A. ferrooxidans* holds considerable potential in biometallurgy, where it efficiently oxidizes ferrous ions and reduced sulfur compounds, thereby promoting the dissolution of metal sulfide ores and facilitating metal extraction and recovery (Dash et al., 2025; Tonietti et al., 2024). In natural ecosystems, this bacterium also contributes to sulfur cycling, helping maintain material balance (Ibáñez et al., 2023; Yi et al., 2023). Environmental pollution has emerged as a critical global issue, with heavy metal contamination posing a particularly severe threat due to its high toxicity to living organisms (Hou et al., 2025; Rahman and Singh, 2019). Arsenic, a highly toxic metalloid, originates from both natural and anthropogenic sources, with the latter significantly accelerating its environmental dispersion. Mining, metallurgy, chemical manufacturing, and other industrial activities release substantial quantities of arsenic-containing waste, leading to severe contamination of soils and water bodies (Bertin et al., 2022; Zhou et al., 2024). Studies indicate that soil arsenic concentrations around many mining areas worldwide are several to tens of times higher than background levels, while in some AMD systems, arsenic can reach hundreds of milligrams per liter (Alekseenko et al., 2025; Irwin et al., 2025; Yang et al., 2024). Many arsenic-resistant microorganisms harbor conserved ars detoxification operons to counteract arsenic toxicity, and multi-omics approaches are widely used to elucidate their adaptation mechanisms (Abdelhadi et al., 2024; Halema et al., 2024, 2026). Such detoxification systems are particularly important for acidophilic microbes inhabiting arsenic-rich acid mine drainage. The acidic habitats preferred by *A. ferrooxidans* frequently overlap with regions of severe arsenic pollution, presenting significant challenges to its survival and functional activity.

Upon exposure to arsenic stress, the iron- and sulfur-oxidizing bacterium *A. ferrooxidans* activates a series of complex adaptive mechanisms to maintain physiological homeostasis. Although previous studies have documented phenotypic alterations in this bacterium under arsenic stress, such as changes in growth rate and cellular morphology (Gao et al., 2018; Zhou et al., 2022), the underlying molecular response mechanisms remain largely uncharacterized. Integrated multi-omics analyses combining transcriptomics, proteomics, and metabolomics offer a powerful approach to unravel the interrelationships among biomolecules and their functions, providing critical insights into complex regulatory networks in organisms (Dar et al., 2023). Transcriptomics captures the dynamic transcriptome profile, revealing genes that are activated or repressed and thus illuminating the immediate gene expression strategies employed by cells in response to environmental stress (Rurek and Smolibowski, 2024). Proteomics directly assesses the abundance, modification, and interactions of intracellular proteins, thereby clarifying functional mechanisms and the overall physiological state of the cell (Guo et al., 2025). Metabolomics enables comprehensive profiling of small-molecule metabolites, reflecting dynamic adjustments in cellular metabolic pathways through changes in metabolite types and concentrations (Huang et al., 2025). These analytical layers are tightly interconnected: the proteome partially represents the functional output of the transcriptome, which itself is modulated by genomic and other regulatory factors (Sanches et al., 2024). By integrating transcriptomic, proteomic, and metabolomic data, the present study comprehensively elucidates the multi-level response mechanisms of *A. ferrooxidans* to arsenic stress. This approach provides novel insights into the interactions between microorganisms and environmental pollutants.

To date, although some progress has been achieved in single-omics studies of *A. ferrooxidans* (Kucera et al., 2025), research on this bacterium under arsenic stress remains limited and lacks systematic integrated multi-omics analysis. The present study employed a combined transcriptomic, proteomic, and metabolomic approach to comprehensively elucidate the molecular response mechanisms of *A. ferrooxidans* under arsenic stress and to evaluate its capacity for heavy metal bioleaching. These findings are expected to advance our understanding of microbial adaptation strategies to heavy metal pollution, optimize biomineralization processes, and provide a theoretical foundation for practical applications in bioremediation and environmental management.

2 Material and methods

2.1 Experimental strain

Acidithiobacillus ferrooxidans BY-3 (*At. f* BY-3; CCTCC-M203071) was isolated from sulfide acid mine drainage in Baiyin, Gansu Province, China, and identified based on 16S rDNA sequence analysis. The strain was routinely cultivated in 9K medium (Su et al., 2025) at 30 °C with orbital shaking at 180 rpm.

The 9K medium was prepared as follows. Basal salts were dissolved in deionized water (per liter: 3.0 g $(NH_4)_2SO_4$, 0.1 g KCl, 0.5 g K_2HPO_4, 0.5 g $MgSO_4{\cdot}7H_2O$, and 0.01 g $Ca(NO_3)_2$), and the solution was autoclaved at 121 °C for 20 min. Separately, 44.78 g of $FeSO_4{\cdot}7H_2O$ was dissolved in deionized water acidified to pH 2.0 with concentrated sulfuric acid and filter-sterilized through a 0.22 μm membrane. The sterile ferrous iron solution was then aseptically added to the autoclaved basal salt solution. The final pH of the complete medium was adjusted to 1.8∼2.5 with concentrated sulfuric acid before use.

2.2 Experimental reagents

RNase-free DNase I, DNA polymerase I, RNase H, Reverse transcriptase and Uracil-N-Glycosylase; Ribo-Zero™ rRNA Removal Kit (Epicenter, Sweden); sodium arsenite (Xiya Reagent, Chengdu); Trizol reagent (Sigma-Aldrich, Shanghai); PrimeScript™ RT reagent Kit for reverse transcription (Cat. No. RR047A) and SYBR® Premix Ex Taq™ II RT-PCR Kit (Cat. No. DRR081A; Takara, Japan); agarose, ethidium bromide and 50× Tris-acetate-EDTA (TAE) (Beyotime Biotechnology Co., Ltd., Shanghai); sodium arsenite (Macklin Biochemical Co., Ltd., Shanghai).

2.3 Arsenic domestication of *At. f* BY-3

Sodium arsenite was used as the arsenic source for domestication of *At. f* BY-3. Cultures pre-adapted to a specific arsenic concentration were inoculated into fresh medium containing a higher arsenic level. Successful domestication at each concentration gradient was defined as the complete oxidation of ferrous iron (Fe^{2+}). The sodium arsenite concentration was progressively increased in sequential steps of 0.2, 0.4, 0.8, and 1.6 g/L. All stages were performed with three biological replicates using a 20% (v/v) inoculum.

2.4 Cell harvesting and total RNA extraction

Acclimated *At. f* BY-3 cells were cultured in media supplemented with 0, 0.8, or 1.6 g/L $NaAsO_2$. For each condition, 2 L of culture was centrifuged at 1,000 rpm and 4 °C for 10 min to remove particulate precipitates such as jarosite. The supernatant was transferred to clean centrifuge tubes and centrifuged at 8,500 rpm and 4 °C for 15 min (Liu et al., 2025). After discarding the supernatant, the bacterial pellets were collected and labeled as C, As1, and As2 (corresponding to arsenic concentrations of 0, 0.8, and 1.6 g/L, respectively) for subsequent proteomic analysis.

2.5 The q-PCR validation

For validation of the transcriptomic data, five up-regulated and five down-regulated differentially expressed genes (DEGs) were selected from the C-VS-As1 and C-VS-As2 comparisons. Gene sequences were retrieved from the National Center for Biotechnology Information (NCBI) Gene database, and specific primers were designed using Premier 6 (Premier Biosoft International, Palo Alto, California, USA) (Table 1). Two stable housekeeping genes, rpoC (RNA polymerase gamma subunit) and rpoB (RNA polymerase beta subunit), were used as internal references for normalization. Quantitative real-time PCR (qRT-PCR) was performed, and relative gene expression levels were calculated using the $2^{-\Delta\Delta Ct}$ method (Chen et al., 2023).

2.6 Protein extraction and peptide digestion

Cell pellets were resuspended in Sample dissolution buffer (SDT) [4% (w/v) Sodium dodecyl sulfate, 100 mM Tris-HCl, pH 7.6], and protein concentration was determined using the Bicinchoninic acid (BCA) assay. Equal amounts of protein (20 μg) were separated on a 4–20% gradient Sodium Dodecyl Sulfate-Polyacrylamide Gel Electrophoresis (SDS-PAGE) gel and stained with Coomassie Brilliant Blue R-250. Gel slices were destained, reduced with 10 mM Dithiothreitol (DTT), alkylated with 55 mM iodoacetamide, and digested with trypsin at an enzyme-to-protein ratio of 1:50 (37 °C, 16 h). The recovered peptides were desalted, lyophilized, and reconstituted in 0.1% (v/v) formic acid (Duong and Lee, 2023).

Peptides were separated on a nanoElute HPLC system coupled to a timsTOF Pro mass spectrometer operating in data-dependent acquisition (DDA) mode with a 60 min linear C18 gradient (mobile phase A: 0.1% formic acid in water; mobile phase B: 0.1% formic acid in 80% acetonitrile; flow rate: 300 nL/min). Raw data were processed using MaxQuant v1.6.14 (Max-Planck-Institute of Biochemistry, Martinsried, Germany) against the *At. f* BY-3 proteome database with the following parameters: trypsin digestion (maximum of two missed cleavages), carbamidomethylation of cysteine as a fixed modification, N-terminal acetylation and methionine oxidation as variable modifications, 20 ppm precursor ion tolerance for the first search, 5 ppm for the main search, 0.05 Da fragment ion tolerance, and 1% false discovery rate (FDR) at both peptide and protein levels. The match-between-runs option was enabled for label-free quantification (Gomez-Zepeda et al., 2024).

2.7 Metabolite extraction

Cell pellets were slowly thawed on ice. A total of 50 mg of bacterial pellet was mixed with pre-cooled methanol/acetonitrile/water solution, sonicated at low temperature for 30 min, and allowed to stand for 10 min. The mixture was then centrifuged at 14,000 g and 4 °C for 20 min. The supernatant was vacuum-dried, re-solubilized in 100 μL acetonitrile aqueous solution by vortexing, centrifuged for 15 min, and the resulting supernatant was collected for mass spectrometric analysis (Holman et al., 2014).

2.8 Data acquisition of LC-MS/MS

Following lysis, total protein was extracted from bacterial pellets and quantified. Proteins were reduced and alkylated to disrupt higher-order structures and then subjected to overnight tryptic digestion. The resulting peptide mixtures were desalted using a C18 column and vacuum-dried to obtain purified peptides (Gomez-Zepeda et al., 2024). Peptides were subsequently separated on a nanoElute nano-flow high-performance liquid chromatography (HPLC). Mobile phase A consisted of 0.1% formic acid in water, and mobile phase B consisted of 80% acetonitrile containing 0.1% formic acid. Separation was performed over a 60 min gradient at a flow rate of 300 nL/min. Eluted peptides were analyzed on a timsTOF Pro mass spectrometer in data-dependent acquisition (DDA) mode. Raw MS data were processed using MaxQuant software against the protein database of *At. f* BY-3 for protein identification and label-free quantification. Search parameters included tryptic digestion, fixed and variable modifications, appropriate mass tolerance values, and a 1% false discovery rate (FDR) threshold for data quality control and protein quantification.

2.9 Integrated multi-omics computational pipeline

Proteomic and metabolomic data were integrated using a multi-step computational workflow. Standardized screening

TABLE 1 Primer design of q-PCR.

Gene	Primer sequence	Product length (bp)	Tm
AFE_RS 10685	5′-AGGCATAGCAGAACTAAACA3′ 5′-ATCTTGCTCCGTATCGCTCA3′	160	50.4 °C 58.3 °C
AFE_RS 13045	5′-CCTTTATGAGGGTCGCAGAG3′ 5′-ATCGAACCAAACATGGGATG3′	144	57.4 °C 57.8 °C
AFE_RS 08365	5′-CCCAGCACCGAGTTTCCATC3′ 5′-TCCCGTAACCCGTGTATTTT3′	124	62.5 °C 57.3 °C
AFE_RS 08360	5′-GGCAGCAAGACCAAGCAAGT3′5 ′-TTGATGGAGCTGATCGAGGG3′	158	60.2 °C 60.6 °C
AFE_RS 03555	5′-TCCAAGATCCAGAGCGTCTA3′ 5′-GTCTCACAACACCGAAGGAA3′	141	55.5 °C 55.5 °C
AFE_RS 00885	5′-ATTATGCCTGAGAATGACCG3′ 5′-GGGCCTCACAGAAGAAATGA-3	128	55.1 °C 57.3 °C
AFE_RS 02475	5′-ACTGGTTCACTAACGGCTAC3′ 5′-GGTCTTCCTTGGGTTTCTTC3′	201	51.9 °C 55.3 °C
AFE_RS 03975	5′-GCATTTCGCCATTATTTGTA3′ 5′-CTTCTCCTTCCAGCGTGATT3′	104	54.3 °C 56.8 °C
AFE_RS 09120	5′-AAAGTTCCCACCCACTGATT3′ 5′-TCTTGGCACTCTTGCTGTTC3′	252	55.8 °C 56.0 °C
AFE_RS 07725	5′-CCAGAATGTTGTGGACGGTAAG3′ 5′-CCGCCCTTTGGGTTTGTA3′	131	55.6 °C 57.5 °C

criteria were applied to identify differentially expressed genes (DEGs), differentially expressed metabolites (DEMs), and differentially expressed proteins (DEPs): molecules with an adjusted p-value < 0.05 and $|\text{fold change}| > 1.5$ were considered significantly altered. FDR correction was applied for multiple testing in the transcriptomic differential expression analysis. Hierarchical clustering and principal component analysis (PCA) were performed on the global gene expression matrix, with cumulative variance explained by the principal components and intra-group sample clustering used as quality control criteria. Sequencing quality control metrics included clean reads, Q20, Q30, GC content, and genome mapping rate. All samples met the quality thresholds: $\geq$6 G effective data per sample, Q20 $>$ 98%, Q30 $>$ 93%, inter-group GC content variation $<$ 3%, and genome mapping rate $\geq$85%.

These DEPs and DEMs were first mapped to shared Kyoto Encyclopedia of Genes and Genomes (KEGG) pathways using clusterProfiler. Correlation analysis between protein and metabolite abundances was performed using Spearman's rank correlation, with significant correlations defined as $|r| > 0.6$ and adjusted p-value < 0.05. Joint pathway enrichment and network visualization were conducted in MetaboAnalyst 5.0 (McGill University, Montreal, Quebec, Canada) and Cytoscape (Institute for Systems Biology, Seattle, Washington, USA) to identify coordinated regulatory modules linking proteomic and metabolomic changes (Lin et al., 2024).

FDR correction was applied to control false positives in multiple testing, with differential molecules screened using an adjusted FDR < 0.05 and $|\text{FC}| > 1.5$. A 200-permutation test was performed to validate the Orthogonal Partial Least-Squares-Discriminant Analysis (OPLS-DA) model. The model was considered valid when the original model showed $R^2 > 0.8$ and $Q^2 > 0.5$, and all permutation-derived Q^2 values were lower than the original Q^2. Metabolites were annotated according to Metabolomics Standards Initiative (MSI) classification standards. Level 1 identification required a secondary mass spectrum matching score $\geq$0.8 with authentic standards and a retention time deviation $<$0.1 min. Level 2 identification was based on database spectral matching with a score $\geq$0.7.

2.10 Bioleaching experiment analysis of *At. f* BY-3

Ore samples used in this experiment were collected from the Xinjiang Uygur Autonomous Region and Xizang Autonomous Region. The ores were ground into fine powder, purified with hydrochloric acid, rinsed three times with ultrapure water, soaked and washed with absolute ethanol, and sterilized in a high-temperature drying oven to eliminate surface microorganisms and complete sample preparation. Scanning electron microscopy coupled with energy-dispersive X-ray spectroscopy (SEM-EDS) was employed to characterize the micromorphology and elemental composition of the mineral powders. Detection parameters were set at an accelerating voltage of 20 kV and a working distance of 8.5 mm. Surface morphology was observed under secondary electron mode, and energy spectrum signals were collected simultaneously to determine element types and relative contents. Detailed mineral composition data are presented in Table 2.

TABLE 2 Spectral surface scan of ore samples relative element content table.

Element	No. 1 Wt%	No. 1 σ	No. 2 Wt%	No. 2 σ
C	50.37	0.23	30.23	0.43
O	19.66	0.15	8.74	0.14
Fe	16.50	0.10	28.55	0.22
S	9.83	0.06	17.99	0.14
Pb	1.08	0.12	0.84	0.21
Si	1.04	0.02	2.29	0.04
As	0.96	0.04	11.03	0.12
Au	0.37	0.08	0.26	0.12
Cu	0.19	0.04	0.08	0.06
Zn	0.00	0.04	0.00	0.07

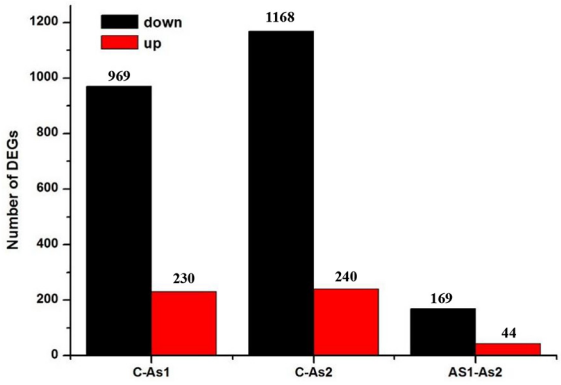


FIGURE 1
Statistical analysis of DEGs under different arsenic domestication concentrations. (C, As1 and As2 represent 0, 0.8 and 1.6 g/L arsenic stress, respectively).

A six-well plate was used to establish the bioleaching system. Six 1 g aliquots of No. 1 ore and six 1 g aliquots of No. 2 ore were prepared separately. To each aliquot, 8 mL of blank medium and 1 mL of either the original or domesticated *At. f* BY-3 suspension were added. Three biological replicates were performed for each treatment. Bioleaching was conducted at 30 °C with shaking at 180 rpm for 24 days. Leachates were sampled on days 12 and 24. After filtration, 50 μL of filtrate was mixed with 1.3 mL of ultrapure water and 150 μL of internal standard solution, and metal concentrations were determined by inductively coupled plasma mass spectrometry (ICP-MS).

3 Results and discussion

3.1 Transcriptomics analysis

Transcriptomic profiling revealed clear molecular responses of *At. f* BY-3 to arsenic stress. In comparisons between the control (C) and low (As1) or high (As2) arsenic concentrations, the total number of differentially expressed genes (DEGs) increased with rising arsenic levels (Figure 1). Down-regulated genes consistently outnumbered up-regulated genes, with 213 DEGs (169 down-regulated and 44 up-regulated) identified in the As1 vs. As2 comparison.

This global transcriptional repression pattern suggests that *A. ferrooxidans* adopts an energy-conserving metabolic strategy under arsenic stress, prioritizing essential survival and detoxification functions over growth and proliferation. Downregulation of non-essential genes likely reduces metabolic burden and reallocates limited resources to stress mitigation pathways, such as those maintaining membrane integrity and redox homeostasis. Similar biases toward down-regulation have been observed in acidophiles exposed to heavy metals or oxidative stress, reflecting a common adaptive shift from anabolic to maintenance metabolism in extreme environments (Li and Wen, 2023). Recent transcriptomic studies support this interpretation. For example, Han et al. (2026) analyzed *A. ferrooxidans* biofilm cells under arsenic stress and identified coordinated regulation of genes involved in extracellular electron transfer, exopolysaccharide biosynthesis, and pilus formation. These findings highlight how arsenic induces targeted transcriptional reprogramming that favors biofilm-mediated protection rather than broad growth promotion.

qPCR validation of 10 selected genes (five up-regulated and five down-regulated from the C vs. As1 and C vs. As2 comparisons) confirmed the reliability of the RNA-Seq data. Although the magnitude of fold changes sometimes differed between qPCR and RNA-Seq owing to the greater sensitivity and specificity of qPCR, the directional trends (up- or down-regulation) were highly consistent (Figure 2). This strong concordance validates the sequencing results and supports their use for downstream functional interpretation. GO enrichment analysis (Figure 3) revealed that the DEGs were primarily associated with catalytic activity, metabolic processes, binding, and cellular components. In the C vs. As1 and C vs. As2 comparisons, significant enrichment was observed in structural molecule activity, RNA binding, carboxy-lyase activity, and aminoacyl-tRNA ligase activity. In contrast, the As1 vs. As2 comparison showed prominent enrichment in intracellular parts, membrane components, and ribonucleoprotein complexes.

These shifts indicate that escalating arsenic concentrations induce membrane remodeling and adjustments in core translational and metabolic machinery. Such changes likely help mitigate toxic metal influx, stabilize intracellular pH and redox balance, and maintain protein homeostasis under increasing stress. The enrichment in membrane-related terms at higher arsenic levels is particularly noteworthy, as it points to enhanced barrier functions and transport regulation, which serve as key defenses against metalloid toxicity. These observations align well with recent multi-omics investigations in *A. ferrooxidans*. Tonietti et al. (2024) reviewed the remarkable versatility of *A. ferrooxidans* in bioleaching and arsenic bioremediation, highlighting its chromosomal arsenic resistance mechanisms and adaptive responses involving membrane transporters and metabolic reprogramming to cope with high arsenic loads in mining environments. Similarly, Liu et al. (2025) demonstrated through arsenic stress experiments and qRT-PCR that arsenic

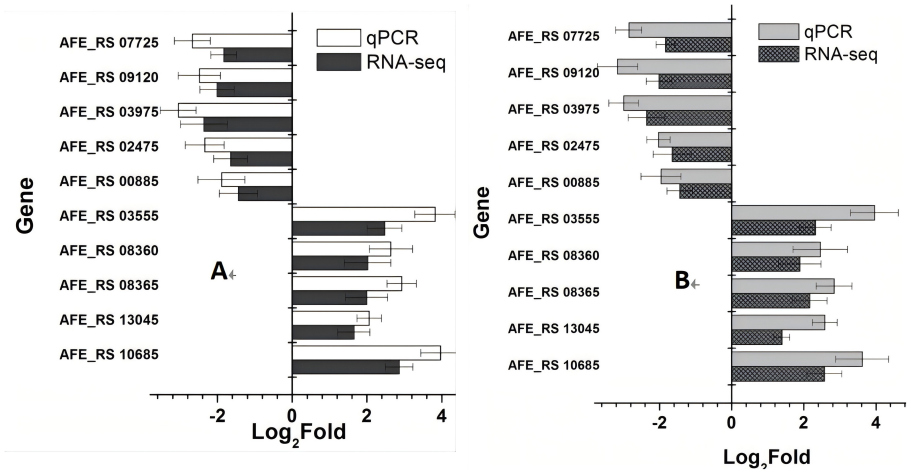


FIGURE 2
Quantitative real-time PCR (qPCR) validation of RNA-Seq transcriptomic data. **(A)** Comparison group C-VS-As1: strains cultured under 0 g/L arsenic vs. 0.8 g/L arsenic; **(B)** Comparison group C-VS-As2: strains cultured under 0 g/L arsenic vs. 1.6 g/L arsenic.

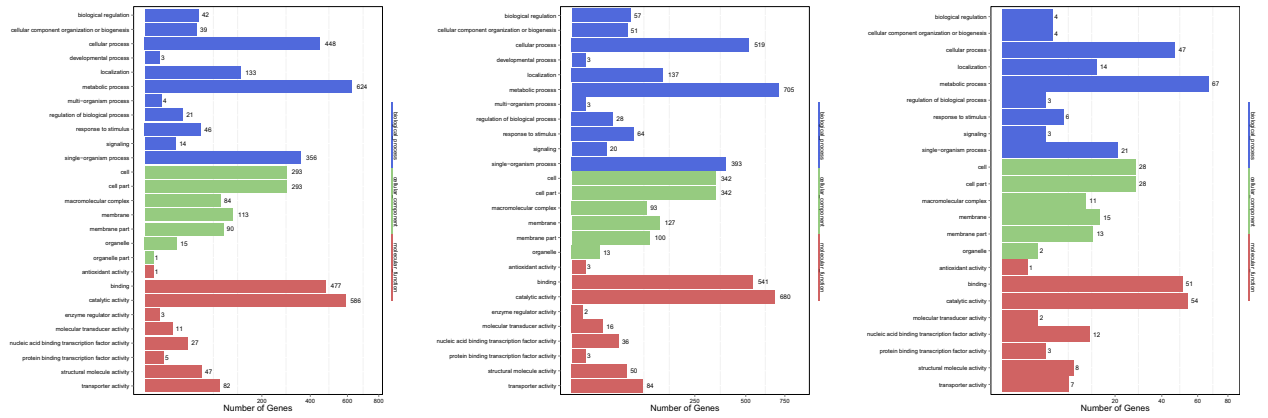


FIGURE 3
GO functional classification of DEGs. **(A)** C-VS-As1; **(B)** C-VS-As2; **(C)** As1-VS-As2.

resistance genes (*ars* operon) are significantly upregulated under bioleaching conditions, supporting the central role of membrane and transport adjustments in tolerance. Nevertheless, the aforementioned studies primarily characterized molecular responses at the transcriptional level. Few investigations have systematically uncovered the multi-layered synergistic regulatory networks during long-term stepwise gradient arsenic acclimation. In contrast to previous reports, the present study utilized a locally isolated and stably long-term acclimated *At. f* BY-3 as the research material and comprehensively elucidated the global molecular regulatory mechanisms of this strain under arsenic stress through integrated transcriptomic, proteomic, and metabolomic analyses.

Furthermore, the observed adjustments in translational machinery (e.g., RNA binding and aminoacyl-tRNA ligase activity) may represent a selective translational control mechanism that ensures efficient synthesis of stress-response proteins while conserving energy—a strategy commonly reported in acidophilic extremophiles under metal stress (Yachkula et al., 2022). In summary, the transcriptomic data indicate a dose-dependent, largely repressive molecular response that promotes cell survival and underpins the proteomic and metabolomic shifts observed in the domesticated strain. These molecular adaptations directly support the improved bioleaching performance, as enhanced stress tolerance enables sustained iron and sulfur oxidation activity even in refractory arsenic-bearing ores. Future targeted gene studies could further elucidate these mechanisms and facilitate strain engineering for industrial applications.

3.2 Proteomics analysis

Proteomic comparison between the original and domesticated *At. f* BY-3 strains identified 337 differentially expressed proteins (DEPs), with 216 up-regulated (105 significantly, $p < 0.05$) and 121 down-regulated (21 significantly; Figure 4). Structural domain enrichment highlighted domains such as N-acyl-L-homoserine

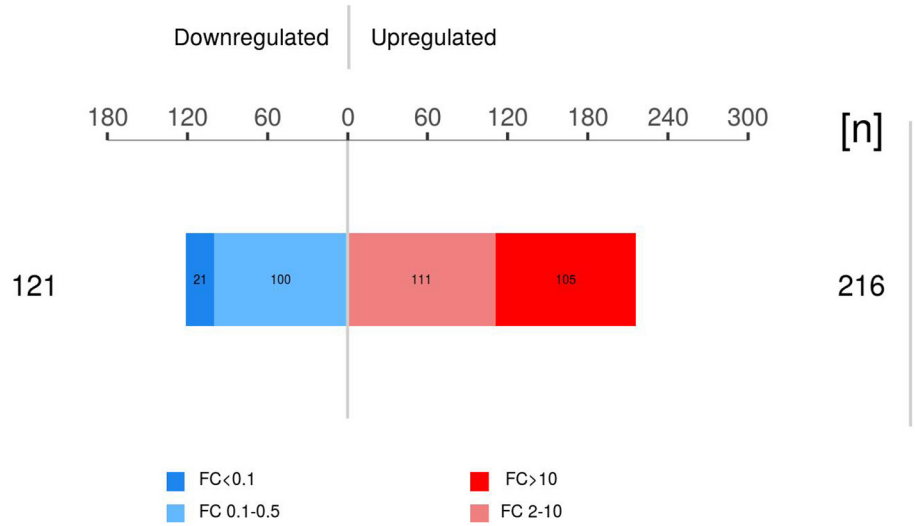


FIGURE 4
Protein quantitation difference histogram.

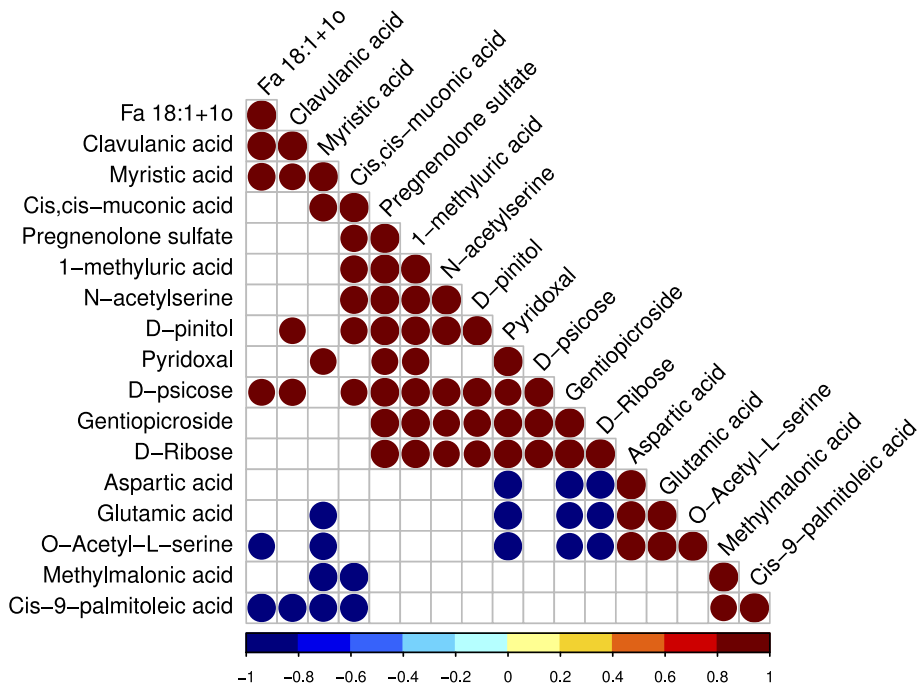


FIGURE 5
Analysis of divergent protein domains **(A)** Prediction of DEPs domains; **(B)** Enrichment analysis of DEPs domains.

lactone amidohydrolase (EAL) and GGDEF-domain protein (involved in c-di-GMP signaling), secretion systems, DNA methylase, hydrogenase-related domains, and porins (Figure 5). These findings indicate enhanced signaling (e.g., regulation of biofilm formation and stress responses via the second messenger c-di-GMP) and improved secretion and metal transport capabilities in the domesticated strain, consistent with mechanisms that promote persistence in metal-rich environments (Bellenberg et al., 2019).

GO annotation (Figure 6A) showed that the DEPs were predominantly associated with metabolic and cellular processes (BP), catalytic activity and binding (MF), and membrane and cell components (CC). Enrichment analysis (Figure 6B) further revealed over-representation in sulfate reduction, secondary metabolite biosynthesis, toxin metabolism, hydrogen sulfide metabolism, heme and oxygen binding, and ferredoxin

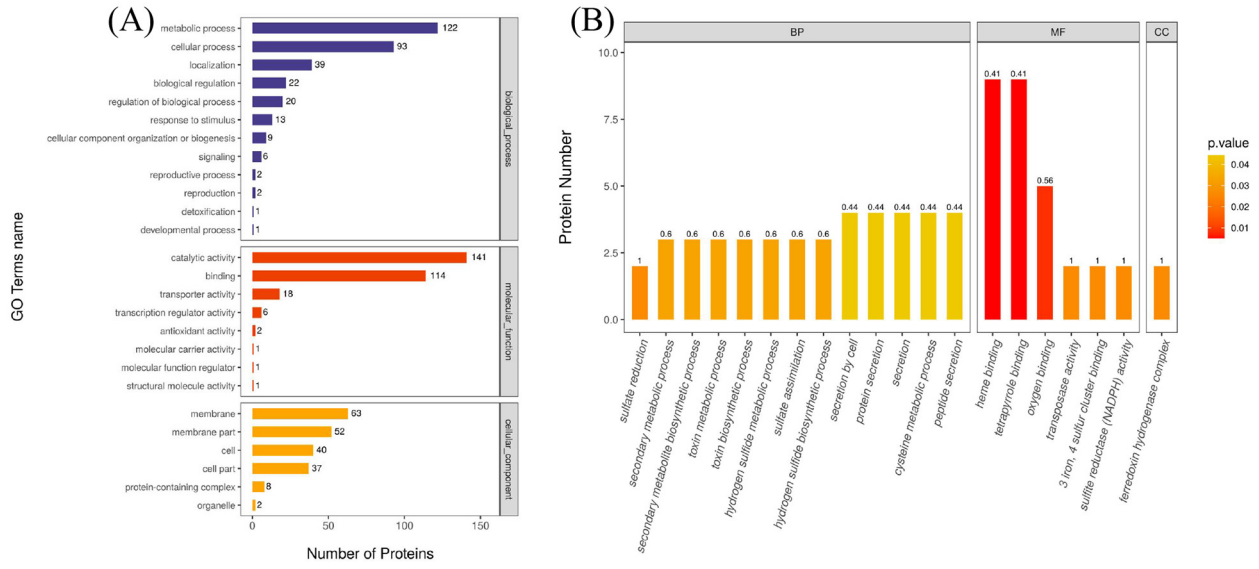


FIGURE 6
Statistical diagram of GO annotation for DEPs. **(A)** GO annotation diagram of the DEPs; **(B)** GO enrichment analysis of the DEPs.

hydrogenase complexes. These results suggest that domestication reprograms central metabolism and redox systems to enhance arsenic tolerance and detoxification capacity, as well as energy conservation pathways critical for efficient bioleaching. The upregulation of sulfur-related processes supports the maintenance of intracellular thiol pools, such as cysteine and glutathione, thereby facilitating metal chelation—a well-documented heavy metal resistance strategy in acidophiles (Shi et al., 2023). Furthermore, the increased abundance of heme/oxygen-binding proteins and hydrogenase complexes supports the optimization of cellular redox homeostasis and electron transfer under combined oxidative and metalloid stress.

KEGG pathway analysis (Figure 7) revealed strong impacts on the two-component system, quorum sensing, glycolysis/gluconeogenesis, pentose phosphate pathway, pyruvate metabolism, and sulfur metabolism. Carbohydrate metabolism accounted for the largest proportion of DEPs (~34%), followed by energy metabolism and signal transduction. This metabolic reconfiguration likely meets the increased energy demands for efflux pumps, repair mechanisms, and exopolysaccharide production, enabling the domesticated strain to maintain high activity under arsenic stress (Ramírez-Aldaba et al., 2026). The prominence of two-component and quorum-sensing pathways underscores coordinated community-level adaptations that are advantageous in bioleaching consortia.

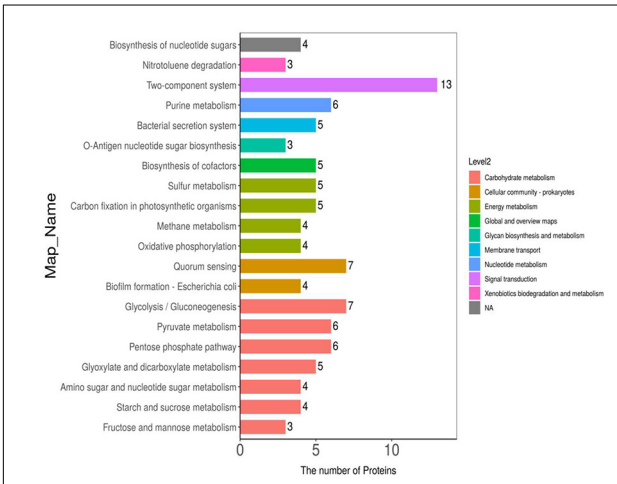


FIGURE 7
Bar chart of KEGG pathway annotations and assignments of DEPs.

3.3 Metabolomics analysis

Multivariate analysis (OPLS-DA) identified 53 differentially expressed metabolites (DEMs), with 33 up-regulated and 20 down-regulated under arsenic stress (Variable Importance in projection (VIP) $>$ 1, $p < 0.05$; Figure 8). These metabolites belonged mainly to organoheterocyclic compounds, organic acids and derivatives, and lipids. Hierarchical clustering (Figure 9) and correlation analysis (Figure 10) revealed coordinated shifts, such as the up-regulation of adenosine and N-acetylserine in the domesticated strain, along with changes in compounds including D-psicose, γ-aminobutyric acid (GABA), and beta-hydroxybutyrate. These patterns suggest adjustments in energy storage, osmoprotection, and signaling metabolites. KEGG pathway enrichment (Figure 11) highlighted ATP-binding cassette (ABC transporters) (the most significantly enriched pathway, involving aspartate, ribose, glutamate, and others), nicotinate and nicotinamide metabolism, sulfur metabolism, butanoate metabolism, and additional pathways. An overall upward trend was observed in pathways such as cAMP signaling and ketone body metabolism, whereas core processes (e.g., amino acid biosynthesis

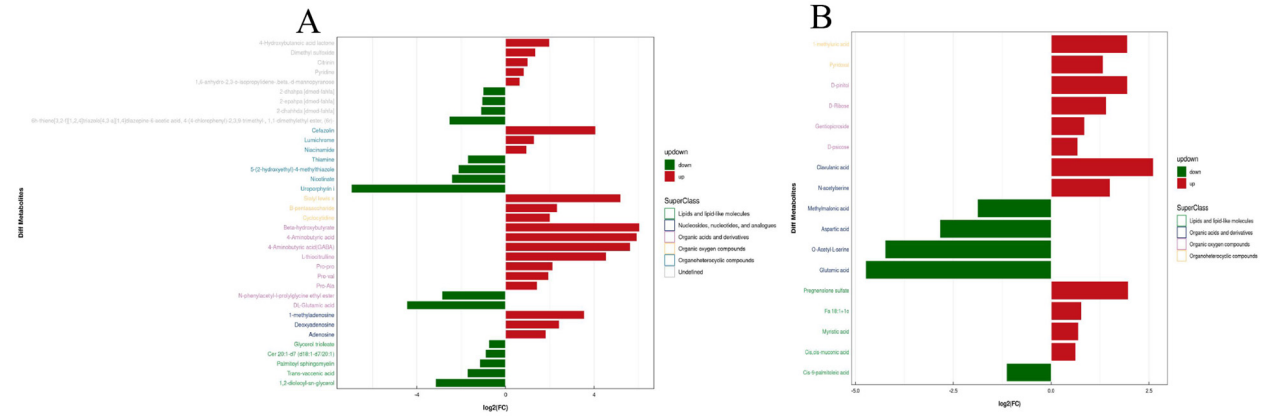


FIGURE 8
Analysis of fold change in expression of significantly DEMs. **(A)** Positive ion mode fold change analysis; **(B)** Negative ion mode fold change analysis.

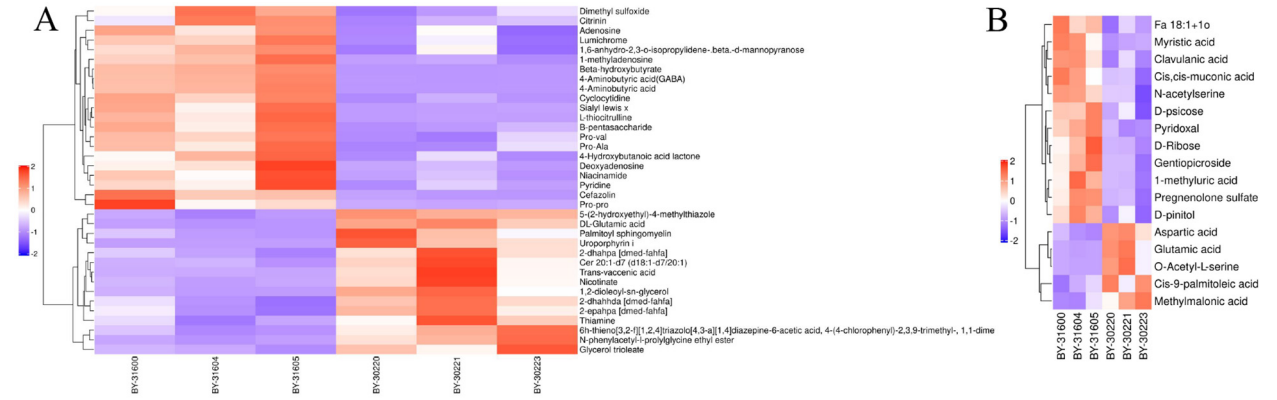


FIGURE 9
Hierarchical clustering heatmap of significantly DEMs. **(A)** Positive ion mode; **(B)** Negative ion mode.

and carbon metabolism) exhibited mixed or downward trends (Dash et al., 2025).

Significant enrichment of the ABC transporter pathway indicates that the strains achieve arsenic detoxification by enhancing the uptake and efflux of intracellular metabolites while ensuring efficient nutrient acquisition. Integrated multi-omics analyses demonstrate that arsenic domestication fine-tunes central carbon and sulfur metabolic fluxes to establish a dynamic balance between alleviation of stress damage and maintenance of bioleaching capacity. The metabolomic reprogramming observed in this study is generally consistent with recent reports on the physiological adaptation of *A. ferrooxidans*, yet it also reveals substantial distinctions and extensions. Wang et al. (2024) conducted combined transcriptomic and metabolomic analyses of *A. ferrooxidans* under electroautotrophic and chemoautotrophic conditions, identifying numerous DEPs involved in galactose metabolism, extracellular polymeric substance (EPS) biosynthesis, and energy metabolism. In contrast, the present study, which focuses on arsenic domestication, observed prominent enrichment in ABC transporter pathways and sulfur metabolism-related metabolites. These alterations corroborate Wang et al.'s findings regarding metabolic reprogramming for energy metabolism and EPS formation, while further uncovering the critical contributions of transporter-mediated detoxification and optimized sulfur metabolic fluxes to sustaining intracellular redox homeostasis under arsenic stress. In addition, Tonietti et al. (2024) highlighted the central roles of membrane transporters and sulfur metabolism in arsenic detoxification and metal mobilization. The present study validates and extends this perspective: metabolites associated with ABC transport and sulfur metabolism were markedly upregulated in the domesticated strain, thereby enhancing detoxification capacity, preserving redox equilibrium, and supporting persistent high-efficiency iron and sulfur oxidation. These results provide experimental and quantitative evidence for the adaptive mechanisms of acidophiles in high-arsenic environments.

Overall, the metabolomics data reveal a finely tuned adaptive strategy in the domesticated *At. f* BY-3, in which enhanced transport, signaling (e.g., cAMP), and thiol/redox-supporting metabolites collectively mitigate arsenic toxicity while preserving bioleaching efficiency. When integrated with the transcriptomic downregulation of genes involved in secondary metabolism and the proteomic upregulation of redox and signaling proteins, these findings demonstrate multi-layered coordinated regulation that facilitates stress-adaptive domestication of the strain. These

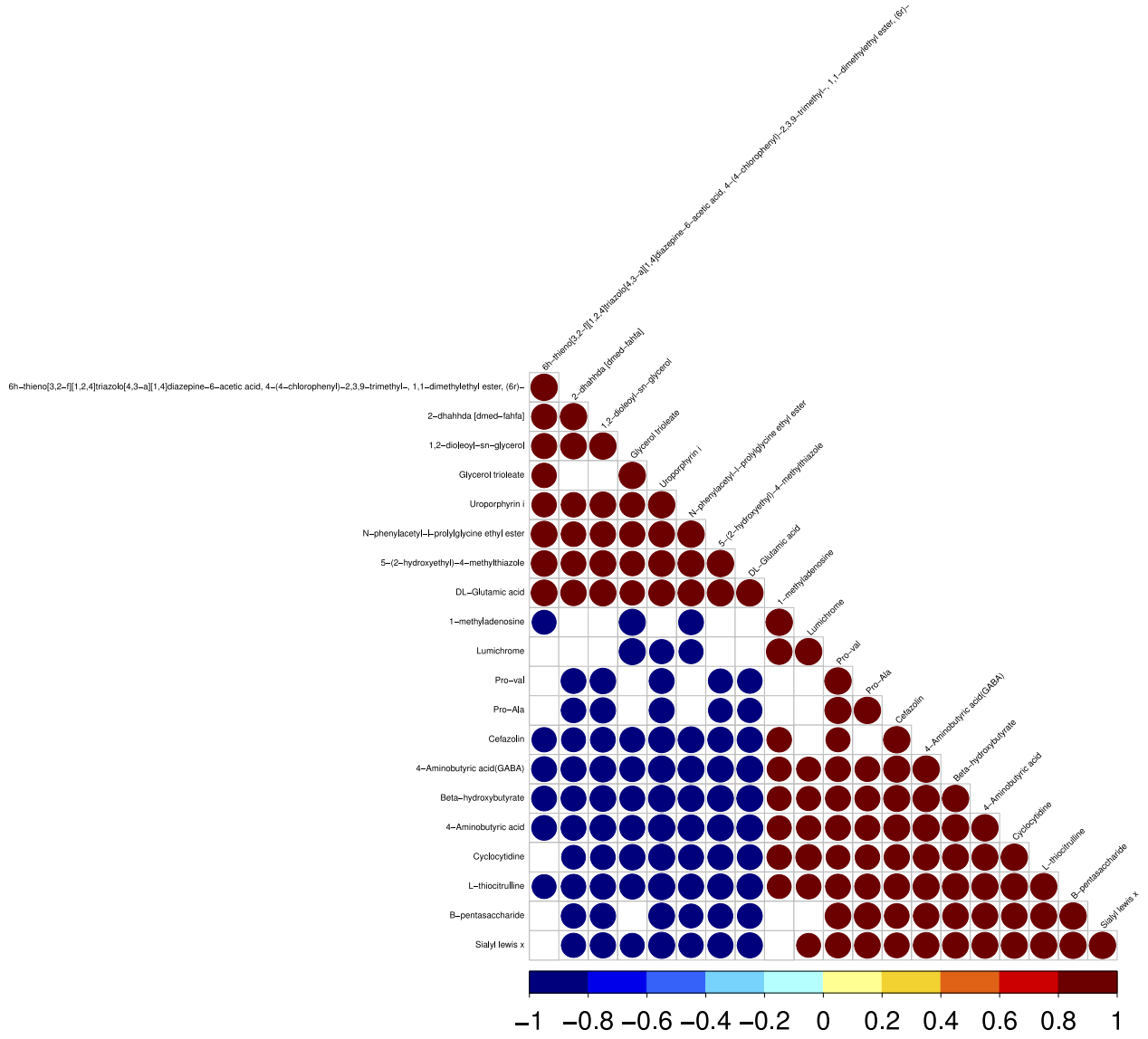


FIGURE 10
Correlation heatmap of DEMs. **(A)** Positive ion mode correlation heatmap; **(B)** Negative ion mode correlation heatmap.

integrated multi-omics results advance our understanding of the physiological mechanisms underlying arsenic stress responses in acidophiles.

3.4 Integrative proteome-metabolome analysis

Information on differential metabolites and differential proteins retrieved from the KEGG database is presented in Table 3. The metabolite compound ID C00025 corresponds to the largest number of associated proteins, including glutamate decarboxylase (WP_054609071.1), Asp-tRNA(Asn)/Glu-tRNA(Gln) amidotransferase subunit GatA (WP_012536979.1), aminodeoxychorismate/anthranilate synthase component II (WP_009567142.1), glutamate-tRNA ligase (WP_012536128.1), and glutamine-fructose-6-phosphate transaminase (isomerizing; WP_012537653.1). The compound ID C00049 ranks second, with associated proteins consisting of aspartate 1-decarboxylase (WP_012537587.1), argininosuccinate synthase (WP_009562807.1), and glutamate decarboxylase (WP_054609071.1).

Integrative analysis was performed on the data for differential metabolites and their corresponding proteins. Figure 12A shows the fold changes of the top 20 groups of differential metabolites paired with differentially expressed proteins ($p < 0.05$). Single-omics enrichment analyses were conducted separately for the metabolome and proteome, with results presented in Figure 12B. The proteome-metabolome integrative enrichment analysis revealed that both differential metabolites and differential proteins were significantly enriched in multiple KEGG pathways, including the pentose phosphate pathway, sulfur metabolism, two-component system, carbon fixation in photosynthetic organisms, and beta-alanine metabolism.

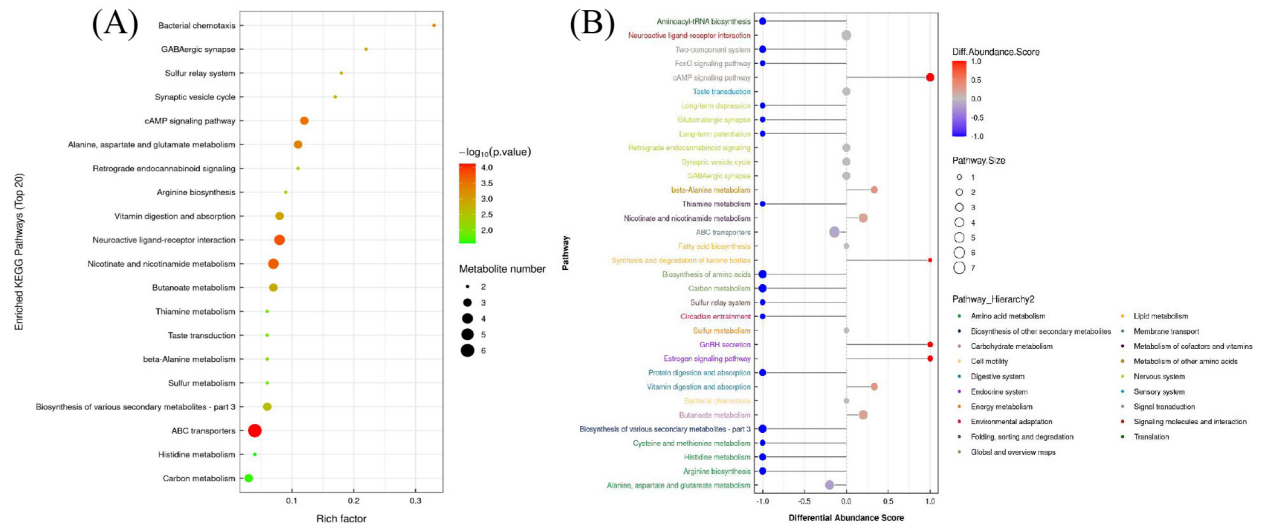


FIGURE 11
KEGG enrichment pathways of DEMs. **(A)** KEGG enrichment map of DEMs; **(B)** Graph showing the differential abundance scores of enriched metabolic pathways.

TABLE 3 Differential metabolites and related proteins information sheet.

Metabolics compound ID	Protein ID	Metabolics description	EC	KO
C00334	WP_054609071.1	4-aminobutyric acid	4.1.1.15	K01580
C00025	WP_054609071.1	Glutamic acid	4.1.1.15	K01580
C00025	WP_012536979.1	Glutamic acid	6.3.5.6	K02433
C00025	WP_012536128.1	Glutamic acid	6.1.1.17	K01885
C00025	WP_009567142.1	Glutamic acid	4.1.3.27	K01658
C00025	WP_012537653.1	Glutamic acid	2.6.1.16	K00820
C00025	WP_012536979.1	Glutamic acid	6.3.5.7	K02433
C00212	WP_009562805.1	Adenosine	2.4.2.1	K09913
C00153	WP_009562805.1	Niacinamide	2.4.2.1	K09913
C00253	WP_009562805.1	Nicotinate	2.4.2.1	K09913
C00559	WP_009562805.1	Deoxyadenosine	2.4.2.1	K09913
C00049	WP_009562807.1	Aspartic acid	6.3.4.5	K01940
C00049	WP_012537587.1	Aspartic acid	4.1.1.11	K01579
C00049	WP_054609071.1	Aspartic acid	4.1.1.15	K01580

3.5 Analysis of the leaching and seepage gold ore effect of *At. f* BY-3

3.5.1 Morphology and elemental analysis of ore powder samples

The EDS morphologies of the two minerals are shown in Figures 13A, B, respectively. Two testing positions were selected for each mineral, and fixed-point electron beam scanning was performed for qualitative and quantitative elemental analysis. The results are presented in Figures 13C, D. Both minerals are primarily composed of C, N, O, S, Fe, and other elements. The relative contents of each element in the two minerals are summarized in Table 4.

The surface of the ore samples was subjected to electron beam surface scanning, with elemental distribution displayed according to brightness (higher brightness indicates higher elemental content). Figures 13A, B show high-resolution EDS elemental mapping images, which intuitively illustrate the differences in elemental distribution within the two ore samples. Combined with the data in Table 2, both ore samples were found to contain various metal elements, including Fe, Pb, As, Au, and Cu.

These features are characteristic of arsenic-bearing refractory gold ores, in which gold is often encapsulated within arsenopyrite

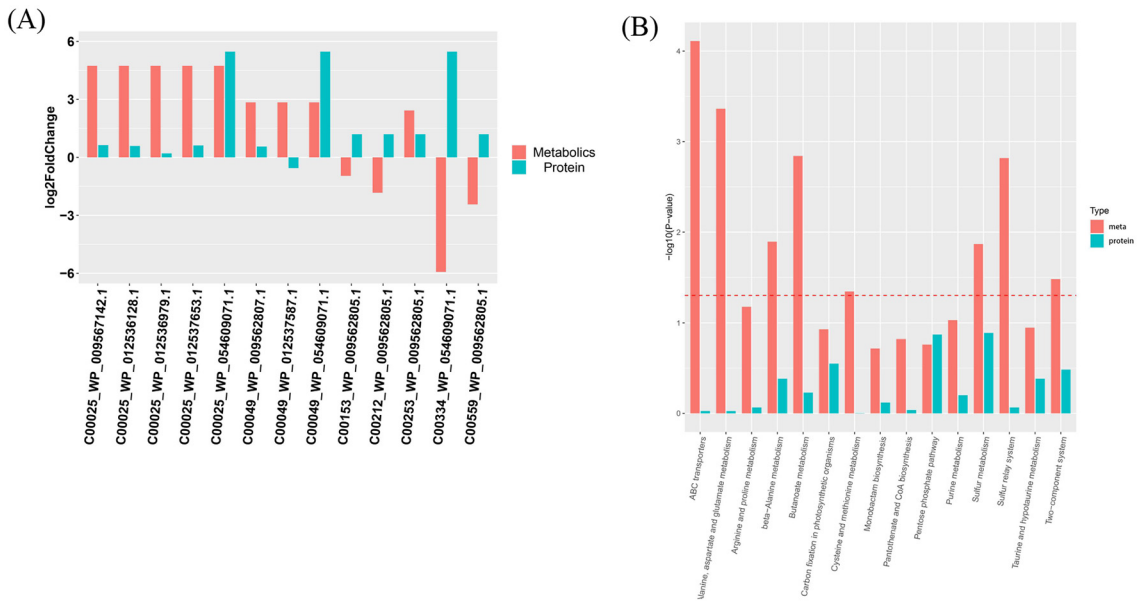


FIGURE 12
Integrative proteomics-metabolomics analysis. **(A)** Expression patterns of DEMs and their associated proteins; **(B)** Bar plot of integrative KEGG enrichment based on proteome and metabolome data.

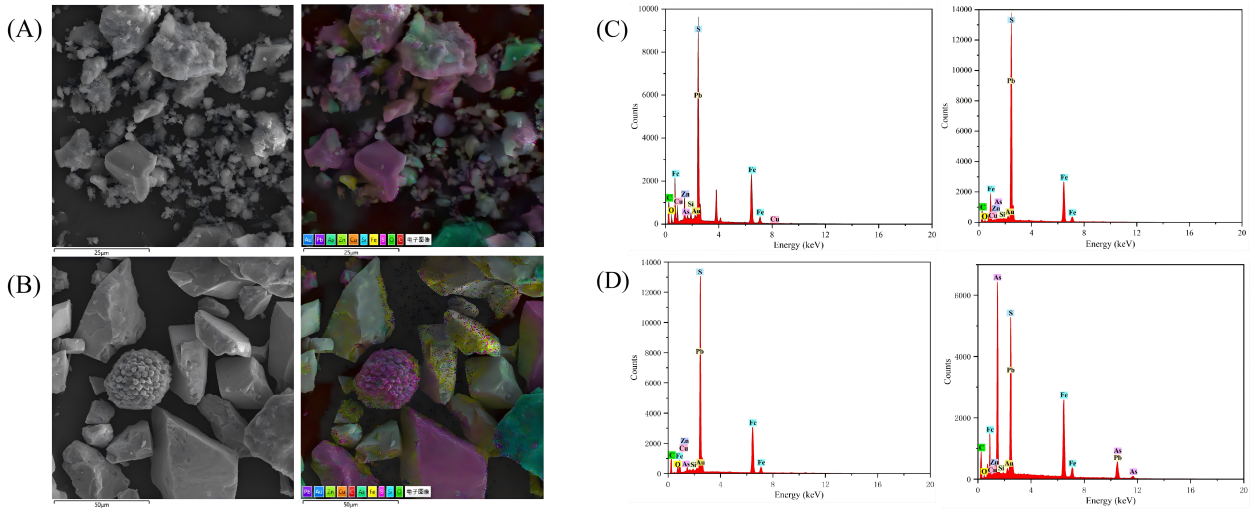


FIGURE 13
Mineral sample analysis **(A, B)** for energy spectrum scanning of ore 1 and 2; **(C)** elemental map of ore 1 obtained by scanning two points on the energy spectrum; **(D)** elemental map of ore 2 obtained by scanning two points on the energy spectrum.

or pyrite matrices, necessitating effective oxidative pretreatment for liberation.

3.5.2 Elemental variations in leachate

ICP-MS analysis of leachates collected on days 12 and 24 revealed that the domesticated *At. f* BY-3 strain exhibited markedly superior arsenic bioleaching performance compared with the original strain for both ore sample 1 and ore sample 2 (Figure 14). These results demonstrate that arsenic domestication substantially enhances the strain's arsenic tolerance and sustained oxidative activity during prolonged bioleaching. The intrinsic molecular mechanisms underlying the improved performance can be explained by the physiological regulatory alterations identified across multiple omics layers in this study. Transcriptomic downregulation of genes involved in secondary metabolism, proteomic enrichment in c-di-GMP signaling (GGDEF/EAL domains), sulfur metabolism, hydrogenases, and membrane transporters, together with metabolomic enhancement of ABC transporters and sulfur-related metabolites, enable the domesticated strain to maintain robust Fe(II) and sulfur oxidation while effectively mitigating arsenic toxicity and secondary mineral passivation.

These findings align closely with recent studies on arsenic-adapted acidophiles. Liu et al. (2025) investigated the biooxidation of arsenopyrite by *Acidithiobacillus ferriphilus* QBS 3 and specifically referenced *At. f* BY-3, reporting that arsenic domestication significantly increases As(III) tolerance (up to 4.74 g/L) and enhances leaching efficiency. Their results confirm that domestication strengthens arsenic resistance mechanisms, including components of the *ars* operon, and improves arsenopyrite oxidation rates, directly supporting the superior performance of the domesticated *At. f* BY-3 observed in the present study. Furthermore, Chen et al. (2025) examined the different fates of Sb(III) and Sb(V) during biogenic jarosite formation mediated by *A. ferrooxidans*. They demonstrated how iron-oxidizing bacteria influence metal(loid) speciation, mobility, and incorporation into jarosite under acidic conditions. This is highly relevant to the current study, as it helps explain how the domesticated *At. f* BY-3 achieves higher metal extraction efficiencies while managing arsenic release and secondary mineral formation during bioleaching of complex ores.

In summary, the integration of multi-omics data with bioleaching experiments confirms that arsenic domestication is an effective strategy for enhancing *At. f* BY-3 performance. Following domestication, *At. f* BY-3 not only withstands elevated arsenic concentrations but also significantly improves arsenic bioleaching efficiency from refractory ores. In this study, the contributions of chemical acid leaching and microbially mediated arsenic release were distinguished based on arsenic leaching results from blank controls and different strain treatment groups. Dynamic monitoring of Fe^{2+} and Fe^{3+} concentrations would further strengthen mechanistic interpretation from the perspective of iron-oxidizing metabolism. This approach holds strong potential for industrial biohydrometallurgy, particularly in the pretreatment of arsenic-rich refractory gold ores to facilitate subsequent gold recovery. Future work should focus on pilot-scale validation and consortia applications to maximize commercial viability.

TABLE 4 Elemental relative content table from spectral point scanning of sample.

Element	Spectrum 1 Wt%	Spectrum 1 At%	Spectrum 2 Wt%	Spectrum 2 At%
(No. 1)				
C	22.52	41.28	14.47	34.81
O	22.33	30.74	3.93	7.09
Si	0.75	0.58	0.21	0.22
S	23.89	16.41	43.12	38.85
Fe	25.05	9.88	36.13	18.69
Cu	0.03	0.01	0.00	0.00
Zn	0.20	0.07	0.06	0.03
As	2.53	0.74	0.12	0.05
Au	0.33	0.04	0.51	0.07
Pb	2.37	0.25	1.46	0.20
(No. 2)				
C	7.01	19.45	7.92	25.05
O	4.97	10.36	5.81	13.79
Si	0.39	0.47	0.22	0.29
S	42.20	43.89	18.19	21.55
Fe	41.11	24.55	29.69	20.20
Cu	0.00	0.00	0.00	0.00
Zn	0.00	0.00	0.00	0.00
As	2.04	0.91	37.45	18.99
Au	0.73	0.12	0.00	0.00
Pb	1.54	0.25	0.72	0.13

4 Conclusion

(1) Multi-omics results revealed profound molecular reprogramming in the strain following arsenic domestication. Transcriptomic data demonstrated a dose-dependent increase in the number of differentially expressed genes, with the strain adopting an energy-conserving metabolic strategy primarily through downregulation of genes related to secondary metabolism. Proteomics identified 337 differentially expressed proteins, with notable enrichment in c-di-GMP signaling, sulfur metabolism, redox systems, and membrane transporters. Metabolomics detected 53 differentially expressed metabolites, primarily associated with

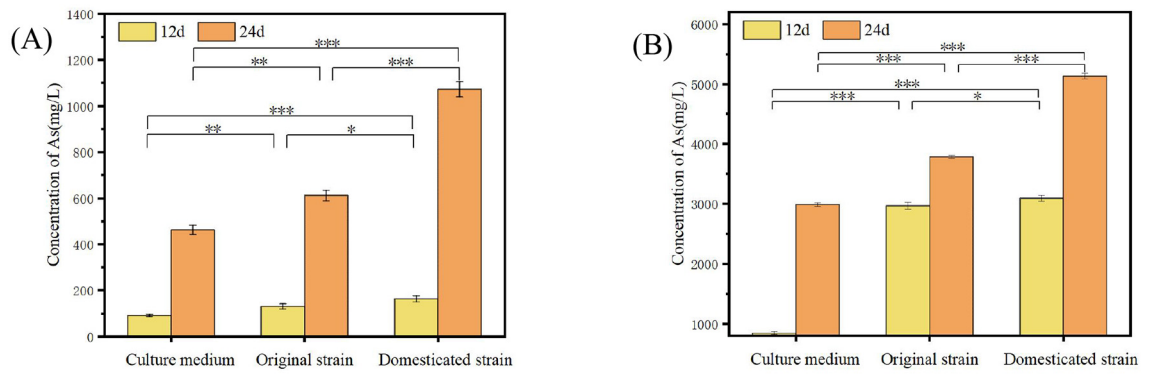


FIGURE 14
Extraction of arsenic from different solution-based mineral powders **(A)** No.1 ore sample; **(B)** No.2 ore sample. *$P < 0.05$, **$P < 0.01$, ***$P < 0.001$.

ABC transporters, sulfur metabolism, and signaling pathways. These coordinated multi-level regulatory changes significantly enhance the arsenic tolerance and overall metabolic activity of the strain.

(2) Bioleaching experiments demonstrated that *At. f* BY-3 possesses robust arsenic bioleaching capacity against refractory gold ores, and domestication further improves the arsenic bioleaching performance of *At. f* BY-3.

This study confirms that arsenic domestication is a simple and effective strain improvement strategy that simultaneously enhances the arsenic tolerance and bioleaching capacity of *A. ferrooxidans*. The domesticated *A. ferrooxidans* exhibits strong application potential in the biological pretreatment of arsenic-bearing refractory gold ores, providing both a theoretical foundation and valuable strain resources for efficient and environmentally friendly biomineralization.

Data availability statement

The data analyzed in this study are publicly available. The transcriptome data are available in the NCBI GEO repository (https://www.ncbi.nlm.nih.gov/geo/query/acc.cgi?acc=GSE350781) under accession number GSE350781. The proteome data are available in the iProX repository (https://proteomecentral.proteomexchange.org/cgi/GetDataset?ID=PXD085594) under accession number PXD085594. The metabolome data are available in the MetaboLights repository (https://www.ebi.ac.uk/metabolights/MTBLS15537) under accession number MTBLS15537.

Author contributions

QG: Writing – original draft. WW: Formal analysis, Validation, Writing – original draft. LX: Investigation, Validation, Writing – original draft. LY: Validation, Writing – original draft. JW: Investigation, Writing – original draft. GX: Funding acquisition, Writing – review & editing.

Funding

The author(s) declared that financial support was received for this work and/or its publication. This work was financially supported by the National Natural Science Foundation of China (82460093), the Science and Technology Research Project Henan Province (222102320325), the Key Research Projects of Higher Education Institutions in Henan Province (24B180011), and Doctoral Research Initiation Fund of Xinxiang Medical University (XYBSKYZZ202125).

Conflict of interest

The author(s) declared that this work was conducted in the absence of any commercial or financial relationships that could be construed as a potential conflict of interest.

Generative AI statement

The author(s) declared that Generative AI was not used in the creation of this manuscript.

Any alternative text (alt text) provided alongside figures in this article has been generated by Frontiers with the support of artificial intelligence and reasonable efforts have been made to ensure accuracy, including review by the authors wherever possible. If you identify any issues, please contact us.

Publisher's note

All claims expressed in this article are solely those of the authors and do not necessarily represent those of their affiliated organizations, or those of the publisher, the editors and the reviewers. Any product that may be evaluated in this article, or claim that may be made by its manufacturer, is not guaranteed or endorsed by the publisher.

References

Abdelhadi, A. A., Elarabi, N. I., Ibrahim, S. M., Abdel-Maksoud, M. A., Abdelhaleem, H. A. R., Almutairi, S., et al. (2024). Hybrid-genome sequence analysis of *Enterobacter cloacae* FACU and morphological characterization: insights into a highly arsenic-resistant strain. *Funct. Integr. Genomics* 24:174. doi: 10.1007/s10142-024-01441-9

Alekseenko, A. V., Machevariani, M. M., Bech, J., and Karthe, D. (2025). Pollution of coal mine soils: global reference concentrations of chemical elements. *Environ. Earth. Sci.* 84:286. doi: 10.1007/s12665-025-12160-0

Bellenberg, S., Huynh, D., Poetsch, A., Sand, W., and Vera, M. (2019). Proteomics reveal enhanced oxidative stress responses and metabolic adaptation in *Acidithiobacillus ferrooxidans* biofilm cells on pyrite. *Front. Microbiol.* 10:592. doi: 10.3389/fmicb.2019.00592

Bertin, P. N., Crognale, S., Plewniak, F., Battaglia-Brunet, F., Rossetti, S., and Mench, M. (2022). Water and soil contaminated by arsenic: the use of microorganisms and plants in bioremediation. *Environ. Sci. Pollut. Res. Int.* 29, 9462–9489. doi: 10.1007/s11356-021-17817-4

Chen, L., Wang, Y., Liu, H., Zhou, Y., Nie, Z., Xia, J., et al. (2025). Different fates of Sb(III) and Sb(V) during the formation of jarosite mediated by *Acidithiobacillus ferrooxidans*. *J. Environ. Sci.* 147, 342–358. doi: 10.1016/j.jes.2023.12.006

Chen, Z., Halford, N. G., and Liu, C. (2023). Real-time quantitative PCR: primer design, reference gene selection, calculations and statistics. *Metabolites* 13:806. doi: 10.3390/metabo13070806

Coleine, C., Delgado-Baquerizo, M., Rosado, A. S., and Zerboni, A. (2025). The role of extremophile microbiomes in terraforming Mars. *Commun. Biol.* 8:1588. doi: 10.1038/s42003-025-08973-1

Dar, M. A., Arafah, A., Bhat, K. A., Khan, A., Khan, M. S., Ali, A., et al. (2023). Multiomics technologies: role in disease biomarker discoveries and therapeutics. *Brief. Funct. Genomics* 22, 76–96. doi: 10.1093/bfgp/elac017

Dash, J., Ojha, R., and Pradhan, D. (2025). Progress in bioleaching and its mechanism: a short review. *Discov. Environ.* 3:238. doi: 10.1007/s44274-025-00454-w

Duong, V. A., and Lee, H. (2023). Bottom-up proteomics: advancements in sample preparation. *Int. J. Mol. Sci*. 24:5350. doi: 10.3390/ijms24065350

Gao, Q., Tang, D., Song, P., Zhou, J., and Li, H. (2018). Bio-adsorption and bio-transformation of arsenic by *Acidithiobacillus ferrooxidans* BY3. *Int. Microbiol*. 21, 207–214. doi: 10.1007/s10123-018-0017-y

Gomez-Zepeda, D., Arnold-Schild, D., Beyrle, J., Declercq, A., Gabriels, R., Kumm, E., et al. (2024). Thunder-DDA-PASEF enables high-coverage immunopeptidomics and is boosted by MS2Rescore with MS2PIP timsTOF fragmentation prediction model. *Nat Commun*. 15:2288. doi: 10.1038/s41467-024-46380-y

Guo, T., Steen, J. A., and Mann, M. (2025). Mass-spectrometry-based proteomics: from single cells to clinical applications. *Nature* 638, 901–911. doi: 10.1038/s41586-025-08584-0

Halema, A. A., Elarabi, N. I., Henawy, A. R., Almutairi, H. H., El-Beltagi, H., Al-Dossary, O., et al. (2026). Genome-based characterization of a multifunctional plant growth-promoting and heavy metal-resistant *Escherichia coli* FACU2024 isolated from Jatropha rhizosphere. *World J. Microbiol. Biotechnol*. 42:297. doi: 10.1007/s11274-026-05029-2

Halema, A. A., El-Beltagi, H. S., Al-Dossary, O., Alsubaie, B., Henawy, A. R., Rezk, A. A., et al. (2024). Omics technology draws a comprehensive heavy metal resistance strategy in bacteria. *World. J. Microbiol. Biotechnol*. 40:193. doi: 10.1007/s11274-024-04005-y

Han, X., Hu, Y., Yue, Y., Ding, Y., Cao, B., Shi, L., et al. (2026). Biofilm engineering through c-di-GMP tuning boosts bioleaching efficiency and arsenic tolerance in *Acidithiobacillus ferrooxidans*. *Appl. Environ. Microbiol*. 92:e0228825. doi: 10.1128/aem.02288-25

Holman, J. D., Tabb, D. L., and Mallick, P. (2014). Employing proteowizard to convert raw mass spectrometry data. *Curr. Protoc. Bioinformatics* 46, 13.24.1–13.24.9. doi: 10.1002/0471250953.bi1324s46

Hou, D., Jia, X., Wang, L., McGrath, S. P., Zhu, Y. G., Hu, Q., et al. (2025). Global soil pollution by toxic metals threatens agriculture and human health. *Science* 388, 316–321. doi: 10.1126/science.adr5214

Huang, H., Chen, Y., Xu, W., Cao, L., Qian, K., Bischof, E., et al. (2025). Decoding aging clocks: new insights from metabolomics. *Cell. Metab*. 37, 34–58. doi: 10.1016/j.cmet.2024.11.007

Ibáñez, A., Garrido-Chamorro, S., Coque, J. J. R., and Barreiro, C. (2023). From genes to bioleaching: unraveling sulfur metabolism in *Acidithiobacillus* genus. *Genes* 14:1772. doi: 10.3390/genes14091772

Irwin, C., Gudka, S., De Meyer, S., Dennekamp, M., Netherway, P., Moslehi, M., et al. (2025). Arsenic in soil: a critical and scoping review of exposure pathways and health impacts. *Environments* 12:161. doi: 10.3390/environments12050161

Kato, T., Guo, Y., Fujimura, R., Nakamura, T., Nishizawa, T., Kurusu, Y., et al. (2022). Complete genome sequence of a *Chemolithoautotrophic* iron-oxidizing bacterium, *Acidithiobacillus ferrooxidans* strain NFP31, isolated from volcanic ash deposits on Miyake-Jima, Japan. *Microbiol. Resour. Announc*. 11:e0100621. doi: 10.1128/mra.01006-21

Kucera, J., Kremser, K., Bouchal, P., Potesil, D., Vaculovic, T., Vsiansky, D., et al. (2025). Proteomic insights into the adaptation of *Acidithiobacillus ferridurans* to municipal solid waste incineration residues for enhanced bioleaching efficiency. *J. Proteome. Res*. 24, 2243–2255. doi: 10.1021/acs.jproteome.4c00527

Li, M., and Wen, J. (2023). Study on the intracellular adaptative mechanism of *Acidithiobacillus caldus* MTH-04 to NaCl stress. *Microb. Cell. Fact*. 22:218. doi: 10.1186/s12934-023-02232-w

Li, S., Zhong, H., Hu, Y., Zhao, J., He, Z., and Gu, G. (2014). Bioleaching of a low-grade nickel-copper sulfide by mixture of four thermophiles. *Bioresour. Technol*. 153, 300–306. doi: 10.1016/j.biortech.2013.12.018

Lin, M., Xu, F., Sun, J., Song, J., Shen, Y., Lu, S., et al. (2024). Integrative multi-omics analysis unravels the host response landscape and reveals a serum protein panel for early prognosis prediction for ARDS. *Crit. Care* 28:213. doi: 10.1186/s13054-024-05000-3

Liu, R., Liu, S., Bai, X., Liu, S., and Liu, Y. (2025). Biooxidation of arsenopyrite by *Acidithiobacillus ferriphilus* QBS 3 exhibits arsenic resistance under extremely acidic bioleaching conditions. *Biology* 14:550. doi: 10.3390/biology14050550

Rahman, Z., and Singh, V. P. (2019). The relative impact of toxic heavy metals (THMs) (arsenic (As), cadmium (Cd), chromium (Cr)(VI), mercury (Hg), and lead (Pb)) on the total environment: an overview. *Environ. Monit. Assess* 191:419. doi: 10.1007/s10661-019-7528-7

Ramírez-Aldaba, H., Ruiz-Baca, E., Escobedo-Bretado, M. Á., García-Montiel, E., Adame-Soto, P. J., and Lara, R. H. (2026). Synergistic mechanisms in the *Acidithiobacillus ferrooxidans* and *thiooxidans* consortium: a comprehensive review. *Environments* 13:216. doi: 10.3390/environments13040216

Rosenberg, E., and Zilber-Rosenberg, I. (2022). Special issue: the role of microorganisms in the evolution of animals and plants. *Microorganisms* 10:250. doi: 10.3390/microorganisms10020250

Rurek, M., and Smolibowski, M. (2024). Variability of plant transcriptomic responses under stress acclimation: a review from high throughput studies. *Acta. Biochim. Pol*. 71:13585. doi: 10.3389/abp.2024.13585

Sanches, P. H. G., de Melo, NC., Porcari, A. M., and de Carvalho, L. M. (2024). Integrating molecular perspectives: strategies for comprehensive multi-omics integrative data analysis and machine learning applications in transcriptomics, proteomics, and metabolomics. *Biology* 13:848. doi: 10.3390/biology13110848

Shi, Y., Wu, W., Yang, Y., Liu, X., Lin, J., Liu, X., et al. (2023). Gene knockout of glutathione reductase results in increased sensitivity to heavy metals in *Acidithiobacillus caldus*. *Front. Microbiol*. 14:1250330. doi: 10.3389/fmicb.2023.1250330

Su, C., Cai, J., Lai, H., Shen, P., and Liu, D. (2025). Novel insights into the modification of chalcopyrite and pyrite by *Thiobacillus ferrooxidans*: surface phase and hydrophilicity studies. *Bioresour. Technol*. 422:132238. doi: 10.1016/j.biortech.2025.132238

Tonietti, L., Esposito, M., Cascone, M., Barosa, B., Fiscale, S., Muscari Tomajoli, M. T., et al. (2024). Unveiling the bioleaching versatility of *Acidithiobacillus ferrooxidans*. *Microorganisms* 12:2407. doi: 10.3390/microorganisms12122407

Wang, M., Yue, Z., Deng, R., She, Z., Zhang, L., Yang, F., et al. (2025). Molecular disruptions in microalgae caused by *Acidithiobacillus ferrooxidans*: photosynthesis, oxidative stress, and energy metabolism in acid mine drainage. *Water Res*. 272:122974. doi: 10.1016/j.watres.2024.122974

Wang, Q., Long, H., Wang, H., and Lau Vetter, M. C. Y. (2024). Characterize the growth and metabolism of *Acidithiobacillus ferrooxidans* under electroautotrophic and chemoautotrophic conditions. *Microorganisms* 12:590. doi: 10.3390/microorganisms12030590

Wu, H., Cui, H., Fu, C., Li, R., Qi, F., Liu, Z., et al. (2024). Unveiling the crucial role of soil microorganisms in carbon cycling: a review. *Sci. Total. Environ*. 909:168627. doi: 10.1016/j.scitotenv.2023.168627

Yachkula, A., Rozova, O., Abashina, T., Vainshtein, M., Grouzdev, D., and Bulaev, A. (2022). Attempts to stimulate leaching activity of *Acidithiobacillus ferrooxidans* strain TFBk. *Minerals* 12:1051. doi: 10.3390/min12081051

Yang, Y., Chen, W., Meng, D., Ma, C., and Li, H. (2024). Investigation of arsenic contamination in soil and plants along the river of Xinzhou abandoned gold mine in Qingyuan, China. *Chemosphere* 359:142350. doi: 10.1016/j.chemosphere.2024.142350

Yi, Q., Wu, S., Liu, Y., Chan, T. S., Lu, Y. R., Saha, N., et al. (2023). Mineral weathering of iron ore tailings primed by *Acidithiobacillus ferrooxidans* and elemental sulfur under contrasting pH conditions. *Sci. Total. Environ*. 856(Pt1):159078. doi: 10.1016/j.scitotenv.2022.159078

Zhou, Y., Huang, W., Nie, Z., Liu, H., Liu, Y., Wang, C., et al. (2024). Fe/S oxidation-coupled arsenic speciation transformation mediated by AMD enrichment culture under different pH conditions. *J. Environ. Sci*. 137, 681–700. doi: 10.1016/j.jes.2023.03.008

Zhou, Y. H., Wang, C., Liu, H. C., Xue, Z., Nie, Z. Y., Liu, Y., et al. (2022). Correlation between Fe/S/As speciation transformation and depth distribution of *Acidithiobacillus ferrooxidans* and *Acidiphilium acidophilum* in simulated acidic water column. *Front. Microbiol*. 12:819804. doi: 10.3389/fmicb.2021.819804